

Electronic Supplementary Information

Two-dimensional Core-shell Donor-Acceptor Assemblies at Metal-Organic Interfaces Promoted by Surface-Mediated Charge Transfer

A. Della Pia^a, M. Riello^b, D. Stassen^c, T. S. Jones^a, D. Bonifazi^{c,d*}, A. De Vita^{b,e*}, and G. Costantini^{a*}

^a Department of Chemistry, University of Warwick, Gibbet Hill Road, Coventry CV4 7AL, UK

^b Department of Physics, King's College London, Strand, London WC2R 2LS, UK

^c Namur Research College (NARC) and Department of Chemistry, University of Namur (UNamur), Belgium B-5000, BE

^d School of Chemistry, Cardiff University, Park Place, Cardiff, CF10 3AT, UK

^e Department of Engineering and Architecture, University of Trieste, I-34127 Trieste, IT

1. Experimental characterization

1.1 Assembly of TCNQ molecules on Au(111)

The deposition of TCNQ on Au(111) results in the formation of an extended H-bonded network of neutral molecules that cover the entire surface (Figure ESI-1(a), α structure)¹, with a rhombic unit cell having dimension: $a_1 = (8.1 \pm 0.1)$ Å, $a_2 = (8.7 \pm 0.2)$ Å, $\alpha = (95 \pm 4)^\circ$. However, closer inspection reveals the presence of few small β -TCNQ aggregates located near monoatomic Au(111) step edges (Figure ESI-1(a), β structure). In particular, the TCNQ molecules arrange with their long axis parallel to the steps, a configuration that maximizes the interaction with the lower part of the step edge, which is electron-rich compared to the upper part and to the flat terrace^{2,3}. This charge accumulation (Smoluchowski effect) locally reduces the electron extraction barrier^{2,4}, enabling the TCNQ molecules to get negatively charged and to arrange in the β phase. Comparison with β assemblies formed by TCNQ in the presence of TBP further illustrates how the driving force for charging TCNQ molecules depends on the combined effects of: (i) the position of the molecular frontier orbitals with respect to the substrate Fermi level; (ii) the electrostatic interaction with the metallic surface; (iii) the electrostatic interaction with neighboring molecules. In a very simplified picture, the positively charged TBP molecules can be thought to promote electron extraction or, equivalently, to induce a "local reduction of the Au(111) local extraction barrier", similar to what is accomplished by the Smoluchowski effect at the lower side of step edges. Preferred nucleation near step edges has also been observed for TCNQ on Cu(111)⁵ and for F₄-TCNQ on Cu(100)⁶ and explained based on the Smoluchowski effect. It should however be noted that, while for these two systems TCNQ acts as an electron acceptor also on flat terraces, this is not true for TCNQ on Au(111). Consistently, STM images of β -TCNQ molecules close to step edges appear identical to those of the small β -TCNQ islands decorated by TBP (Figure 4(c)). In particular, the molecular shape at negative bias voltage resembles the LUMO state lobes of gas phase TCNQ, and shows additional bright protrusions near the nitrogen atoms (Figure ESI-1(c)).

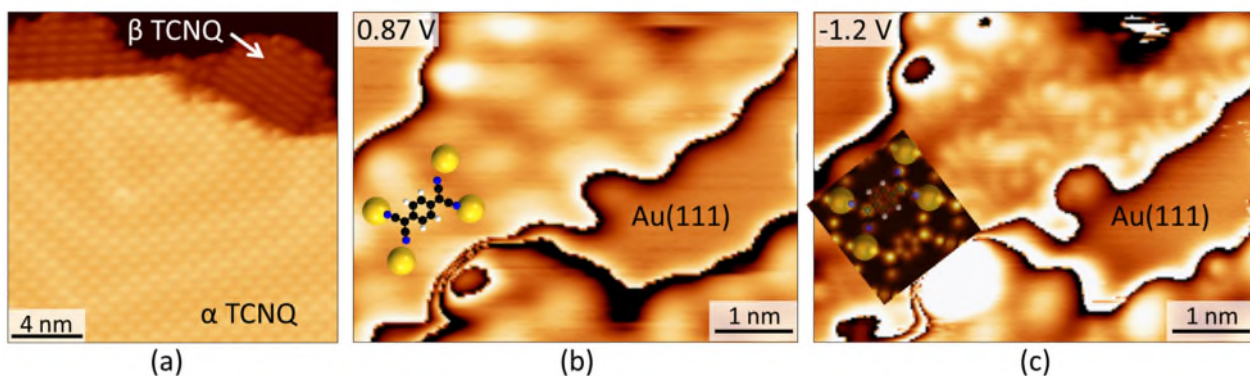


Figure ESI-1: (a) TCNQ molecules on Au(111) assemble in the α structure on the terraces and in the β structure near the lower part of substrate monoatomic steps. (b,c) Tunneling voltage dependence for the β phase observed close to step edges in the case of sole TCNQ deposition at (b) positive and (c) negative voltage, respectively. Structural models are superposed in both images for reference. The inset in (c) reports the simulated STM image at -1.2 V. z offsets have been subtracted in the images at three different threshold values for a better visualization of the molecular features.

1.1 Co-deposition of TBP and TCNQ molecules on Au(111)

When TBP and TCNQ molecules are co-deposited on the Au(111) surface and if TCNQ is in excess, homomolecular α -TCNQ islands coexist with the TBP-decorated β -TCNQ small aggregates, as shown in Figure ESI-2.

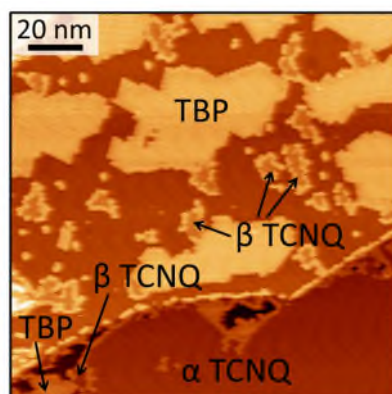


Figure ESI-2: STM images of the assembly resulting from the co-deposition of TBP and TCNQ on the Au(111) substrate, with TCNQ in excess.

1.2 Tunneling spectroscopy experiments on co-deposited TBP and TCNQ molecules on Au(111)

Attempts to perform STS measurements on TBP molecules surrounding β -TCNQ islands usually resulted in a modification of the TBP adsorption configuration, typically in a rotation. Spectra could however be acquired on TBP molecules belonging to TBP homomolecular islands adjacent to β -TCNQ aggregates. Such dI/dV measurements did not show any peak associated to molecular levels, the only evident feature being a shift of (140 ± 10) mV of the surface state onset towards the Fermi level, as visible in Figure ESI-3. A similar shift has been observed for other molecular systems^{7,8} and has been associated with an interfacial charge rearrangement due to the pillow effect or to a chemical bond with the surface. Since TBP does not interact strongly with Au(111)⁹, the measured shift can only be attributed to the pillow effect.

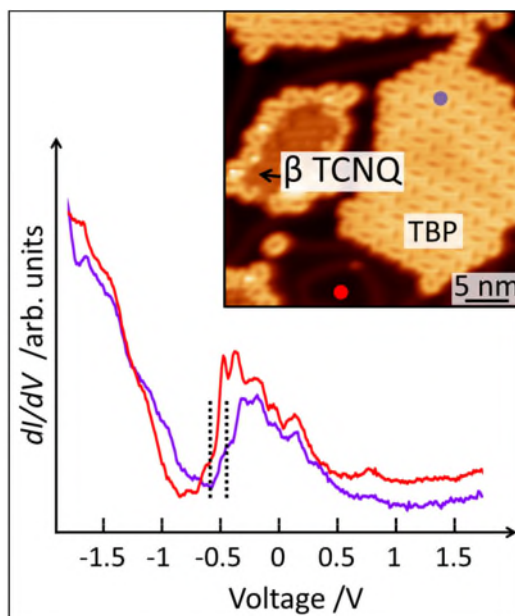


Figure ESI-3: dI/dV spectroscopy performed on TBP molecules (violet curve) and on the clean Au(111) substrate (red curve). The STM image in the inset shows the positions where the two spectra were acquired, indicated by filled circles having the same color as the corresponding spectra.

1.3 Co-deposition of TBP and TCNQ molecules on Cu(111)

In the main paper we describe the co-deposition of TBP (electron donor) and TCNQ (electron acceptor) molecules on the Au(111) substrate where TBP deposited on its own undergoes a CT process and becomes positively charged⁹ but TCNQ alone adsorbs in its neutral charge state¹.

We also investigated the same molecular mixture on a Cu(111) substrate, where the mirror situation occurs: TBP alone adsorbs as a neutral molecule⁹ while TCNQ gets negatively charged¹⁰. Low coverage co-deposition of TBP and TCNQ on Cu(111) held at room temperature yields preferential adsorption of TCNQ molecules at copper monoatomic steps, which act as nucleation sites for the growth of extended islands. These are surrounded by a monomolecular rim of TBP (Figure ESI-4(a)), similar to what observed for the β -TCNQ phase when the two molecules are co-deposited on Au(111). The remaining TBP molecules aggregate into small islands (Figure ESI-4(a)). TCNQ molecules have the same orientation – parallel to the step edges – as when deposited alone on Cu(111)⁵, but form noticeably larger islands in the presence of TBP, which seems to screen the repulsion between the negatively charged TCNQ molecules, thus stabilizing larger β -type parallel assemblies. At higher TCNQ coverage (Figure ESI-4(b)), TCNQ islands increase in size while their borders remain surrounded by a rim of TBP molecules. The molecular assembly within the TCNQ islands does however change, passing from the parallel alignment to a coexistence of several phases whose predominance depends on the annealing temperature, as observed for TCNQ deposited on Cu(111) on its own^{5,11}. Conversely, increasing the TBP coverage, large TBP islands are observed (Figure ESI-4(c)), as in the case of deposition of sole TBP on Cu(111)⁹. Small aggregates of few TBP molecules (up to 4) are sometimes also found on the surface due to nucleation around impurities, as verified by lateral molecular manipulation experiments.

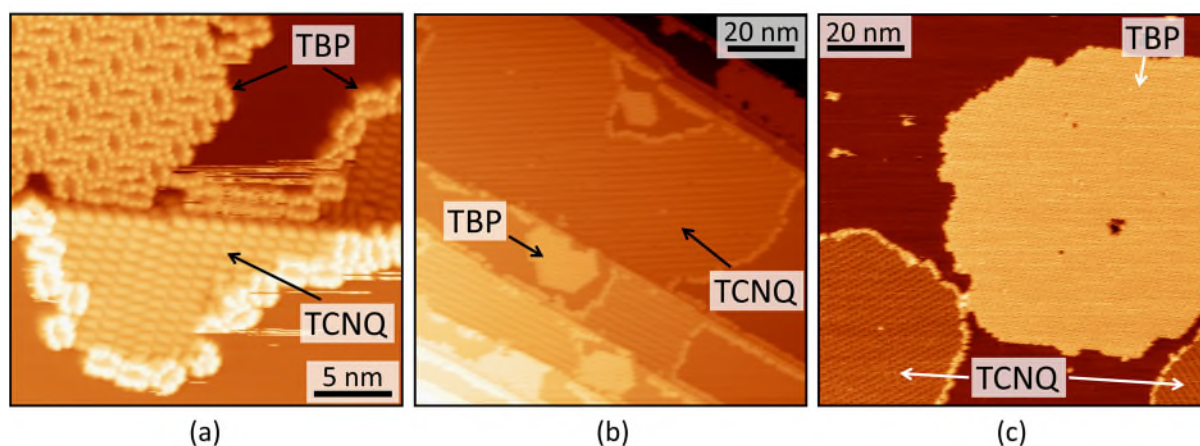


Figure ESI-4: STM images showing the assembly resulting from the co-deposition of TBP and TCNQ molecules on Cu(111) after an annealing to 350 K: (a) at low overall coverage close to step edges; (b) at high TCNQ coverage and low TBP coverage; (c) at high TCNQ and TBP coverage.

At all investigated coverages, TBP molecules first adsorb at the borders of TCNQ islands and only afterwards form TBP homomolecular islands. If TBP molecules were neutral, they would prefer to form homomolecular islands instead of surrounding TCNQ islands, since a neutral TBP molecule would gain a larger amount of energy by binding to another TBP instead of to a TCNQ molecule (see Monte Carlo simulations in Sec. 3 below). On the contrary, a cationic charge state for TBP would explain the observed formation of a TBP rim, as this would be favored by the attractive electrostatic interaction between oppositely charged molecules (oppositely oriented molecular dipoles, when considering the surface image charge¹²). The experimental observations are thus consistent with the assumption that the spatial proximity of negatively charged TCNQ molecules induces the positive charging of TBP even on a surface, Cu(111), where the same molecule adsorbs as a neutral species when deposited on its own⁹. In other words, in a mirror analogy to what reported in the main paper for TCNQ in the presence of TBP on Au(111), here we show that the presence of electron acceptor TCNQ molecules enables the otherwise forbidden donation of charge from TBP to Cu(111). This amounts to further evidence that molecular charging is the result of the combined effect of frontier molecular orbital energy level alignment and electrostatic interaction with the substrate and neighboring molecules.

2. Density functional theory simulations

2.1 TCNQ neutral in the β configuration

We performed DFT calculations on a monolayer of TCNQ molecules in gas phase initially organized in the experimentally determined β configuration. The molecules show a clear tendency to rearrange in less dense α -phase like structures with brickwork H-bonded assembly (Figure ESI-5(a)). Consistently, a significant total energy decrease is obtained by shifting the relative position of the molecules, thereby moving the nitrogen atoms far from each other. DFT calculations performed on the Au(111) surface starting from the experimental configuration furthermore show that the molecules rotate in the plane in order to maximize the distance between the nitrile groups and thus to minimize the repulsion (Figure ESI-5(b)), with the formation of two H-bonds per neighbor.

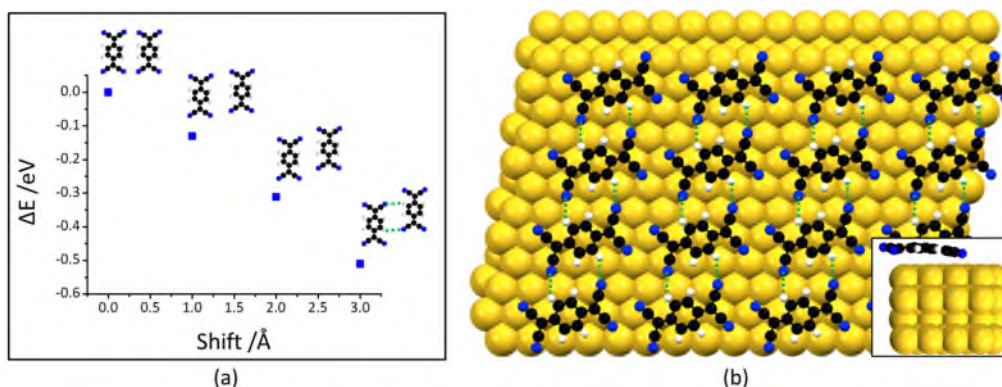


Figure ESI-5: DFT calculations performed on 1 ML of neutral TCNQ molecules in (a) gas phase and (b) adsorbed on Au(111). (a) Plot showing the decrease of total energy (ΔE) upon moving the molecules with respect to each other (shift). For each point in the graph, the monolayer was built by replicating the sketched dimer configuration. (b) The TCNQ molecules adsorb almost flat on the surface, as shown in the inset, and rotate from the initial parallel configuration in order to make H-bonds and reduce electrostatic repulsion. C≡N...H≡C hydrogen bonds are marked by green dashed lines in both images.

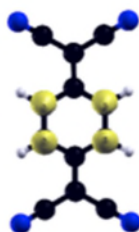


Figure ESI-6: Spatial plot of the LUMO+1 derived resonance of TCNQ, calculated by DTF for a single molecule in gas phase.

2.2 Metal-organic network formed by TCNQ molecules on Au(111)

We considered a complete TCNQ overlayer in the experimental β configuration and incorporated one additional Au adatom for each TCNQ molecule, located in a hollow site of the Au(111) substrate. In the stable metal-organic structure formed (Figure 6(a)), each TCNQ molecule coordinates only to two adatoms, with a bond length of 2.2 Å, to be compared to a Au-N separation of 3.5 Å for the two further adatoms. This difference is primarily due to the different symmetry of the triangular unit cell of the substrate with respect to the rhombic cell of the molecular layer. The rhombic unit cell is defined by the parameters $b_1 = 7.82$ Å, $b_2 = 11.97$ Å and $\theta = 100.9^\circ$, in good agreement with the experimental values $b_1 = (7.3 \pm 0.1)$ Å, $b_2 = (11.1 \pm 0.3)$ Å and $\theta = (98 \pm 2)^\circ$.

The STM simulated image on this metal-organic network at a bias voltage of -1.3 V is reported in Figure ESI-8(b) and resembles well the experimental STM image acquired at the same voltage (Figure 4(c)). The TCNQ molecules appear with a LUMO-like shape and a strong signal localized on the cyano groups. The two cyano groups bound to the Au adatoms appear brighter than the other two, reflecting the asymmetry in the bonds. Finally, additional protrusions, corresponding to the adatoms, are present next to the cyano groups of neighboring molecules.

While the DFT-optimized model with adatoms strongly agrees with all the experimental observations, a model considering some lifting of the substrate atoms could be equally valid. From a structural point of view, the two models are shifted by one substrate lattice vector with respect to each other so that in one case the adatoms are in hollow positions while in the other the atoms are pulled up from the substrate and thus keep their “on top” position. Several examples can be found in the literature where molecular adsorption is reported to induce the extraction of atoms directly from the substrate^{7,13,14} or the segregation of adatoms by lifting of surface reconstructions^{15,16}. In our case, the relatively small size of the β islands, does not allow to determine whether the Au(111) herringbone structure is preserved or not below the molecular assembly. It is thus not possible to ascertain whether the adatoms in the metal-organic structure originate from step edges or from a lifting of the herringbone reconstruction. We do however exclude a direct extraction of atoms from terrace sites, as this would be associated with an excessively high energy cost.

2.3 Charge rearrangement at the metal-organic interface

The pDOS projected onto the molecular states and onto the Au adatom reported in Figure ESI-7(b) gives an insight in the type of metal-organic interaction existing between TCNQ molecules and Au adatoms in the β aggregates. The pDOS onto the Au adatom shows a small peak around -1.2 eV coincident with the molecular pDOS peaks onto the cyano groups and carbon rings associated with the previous gas phase HOMO. This observation points toward a covalent Au-TCNQ bonding, an hypothesis supported by the calculated total electron density pattern revealing the presence of charge on the Au-N sites (Figure ESI-8(a)). As Au is a transition metal, the occurrence of this type of bond is not surprising and has been indeed found in other related systems¹⁷.

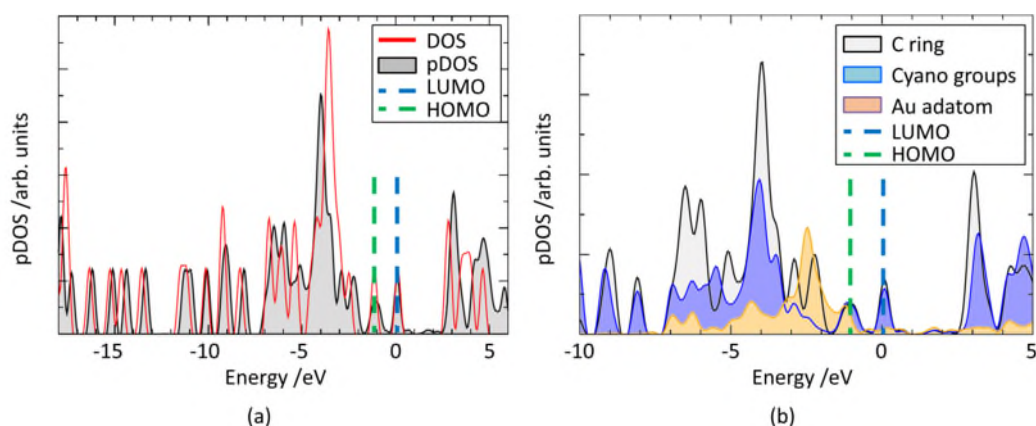


Figure ESI-7: (a) DFT calculated pDOS of TCNQ β phase on Au(111) (filled grey area), compared with the molecular DOS calculated in gas-phase (red line). The gas phase HOMO-LUMO DOS peaks have been aligned with those of the pDOS. The Fermi level E_F of the fully interacting molecule-substrate system is set to zero. (b) pDOS projected onto the N (filled blue area) and C (filled grey area) atom components and onto the Au adatom (filled orange area).

Charge rearrangement at the metal-organic interface have been extracted from DFT calculations by subtracting the charge densities of the isolated subsystems (molecule and substrate) from that of the combined system:

$$\Delta\rho(r) = \rho_{\text{int}}(r) - [\rho_{\text{sub}}(r) + \rho_{\text{mol}}(r)],$$

where $\rho_{\text{int}}(r)$ is the fully interacting electronic density, while $\rho_{\text{sub}}(r)$ and $\rho_{\text{mol}}(r)$ are the substrate and molecule electronic densities separately calculated in the adsorbed atomic geometry (Figure 6(b)).

By integrating $\Delta\rho(r)$ over the x - y plane within a unit cell (thereby obtaining a $\Delta\rho(z)$ distribution), we can get further insight in the charge transfer process (Figure ESI- 8(c)). Namely, a strong dip is resolved on the adatom position and a strong accumulation is observed on the molecule, in particular on the core. A further small charge accumulation is present on the Au slab just underneath the adatom due to screening rearrangement of the charge inside the metal, while the bottom three gold layers do not participate to the CT. The total charge transferred calculated through Bader analysis is $0.54 e^-$, mainly coming from the adatom ($0.46 e^-$) and for a small fraction from the Au(111) surface ($0.08 e^-$).

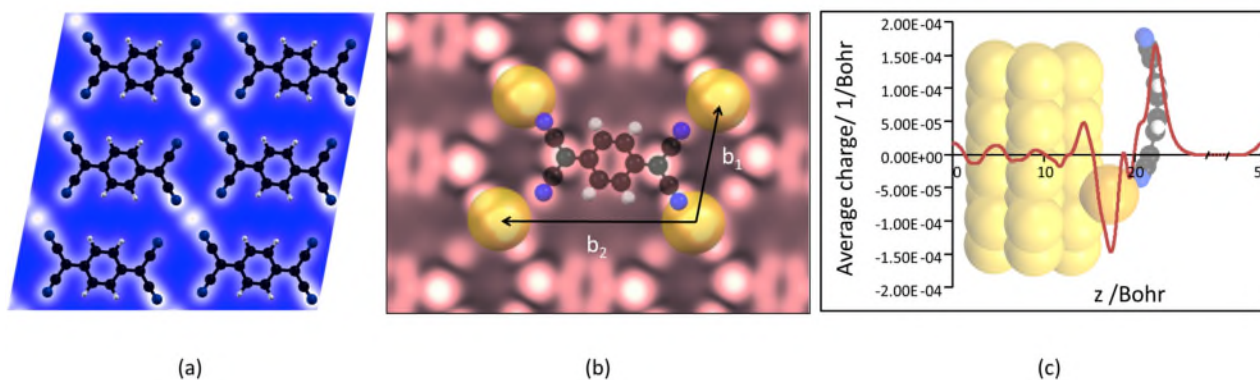


Figure ESI-8: (a) Space-resolved electron density plot for the metal-organic structure shown in Figure 6(a). (b) Constant current STM image at $V = -1.3$ V simulated using the Tersoff-Hamann approach¹⁸ on the metal-organic structure shown in Figure 6(a). (c) Plot of $\Delta\rho(r)$ integrated over the x - y plane within the unit cell, versus the z direction perpendicular to the surface. Positive values correspond to electron accumulation, negative values to depletion.

3. Equilibrium Monte Carlo simulations

In the equilibrium Monte Carlo simulations, we modelled the coexistence of two molecular species treated as structure-less particles, accommodated on a two-dimensional hexagonal lattice. The particles simulating the TBP molecules were associated with a positive dipole pointing away from the surface. For these low-coverage simulations all the TBP molecules were considered charged (i.e., no switching to a neutral status of the TBP molecules was allowed)⁹. The value of the TBP dipole was estimated from standard electrostatics within the image charge approximation and in the integer charge transfer limit (i.e., $p_{\delta=1} = e \times (2 l_D)$, where l_D is the calculated adsorption distance corrected to account for the image plane distance^{19,20}). The particles representing TCNQ molecules were instead supposed to be negatively charged. Since the vertical distance between the molecular core and the adatom is roughly half the adsorption distance of TBP on Au(111), their negative dipole ($p_{\delta=2}$) was set to minus half of the TBP ICT dipole value.

The short-range attractive van der Waals coupling constant for TBP-TBP pairs was calculated at the DFT level (vdW-DF functional²¹). The strong short-range interaction for TCNQ-TCNQ pairs was set to three times the value used for TBP-TBP to account for the metal-organic interaction. Further short-range attractive van der Waals forces between TCNQ-TBP hetero-pairs are expected to be

weaker than those existing between TBP-TBP pairs, because the different chemical nature and adsorption geometry of the two molecules lead to an increase of the bond length. In particular, the TCNQ-TBP coupling was arbitrarily set to half of the TBP-TBP one. Finally, long range electrostatic interactions between all pairs of molecules were modelled with a $1/R^3$ term to model the repulsion between standing dipoles. This implies a screening electrostatic effect originated by the charged TBP molecules and acting on the TCNQ molecules (notably, non-nearest neighbor ones). The Hamiltonian describing the system was:

$$H = -J_k \sum_{\langle i,j \rangle} \sigma_i \sigma_j + \frac{1}{2} \sum_{\substack{i,j \\ i \neq j}} \frac{p(\delta_i) p(\delta_j)}{|\mathbf{r}_i - \mathbf{r}_j|^3} \quad [1]$$

where: i, j are lattice site indexes; σ defines the state occupation ($\sigma = 2$ for a TCNQ-occupied site, $\sigma = 1$ for TBP and $\sigma = 0$ if the site is vacant); J_k is the attractive coupling constant; $\langle i, j \rangle$ are nearest neighbor site pairs; $p(\delta_i)$ is the molecular dipole value at an occupied site i , and δ is a dipole-type flag, set to 1 for cations and 2 for anions; \mathbf{r} is the site position vector.

Table 1 Parameters used in the model Hamiltonian.

J (TBP-TBP)	0.12 eV
p ($\delta = 1$)	10.56 ea_0
p ($\delta = 2$)	5.28 ea_0

The presence of long-range electrostatic energy terms increases the computational cost (which scales as the square of the number of particles) and requires the use of periodic boundary conditions (PBC) to avoid finite size effects. PBC were implemented by direct summation²², re-writing the Hamiltonian in Eq. 1 as:

$$H = \sum_{i,j} \sum_{\mathbf{R}} \left\{ -\left[\Pi(\mathbf{r}_i, \mathbf{R} + \mathbf{r}_j) \sigma_i \sigma_j \right] + \frac{1}{2} \left[\Delta(\mathbf{r}_i, \mathbf{R} + \mathbf{r}_j) p(\delta_i) p(\delta_j) \right] \right\} \quad [2]$$

where \mathbf{R} is a translation vector which transforms the original system in any of its images and the functions Π and Δ accounting for the short-range nearest neighbors (NN) coupling and the repulsion terms, respectively, are defined as:

$$\Pi(\mathbf{r}_i, \mathbf{R} + \mathbf{r}_j) = \begin{cases} J_k & \text{if } \mathbf{r}_i \text{ and } \mathbf{R} + \mathbf{r}_j \text{ are NN,} \\ 0 & \text{otherwise.} \end{cases} \quad [3]$$

$$\Delta(\mathbf{r}_i, \mathbf{R} + \mathbf{r}_j) = \begin{cases} 0 & \text{if } \mathbf{r}_i = \mathbf{R} + \mathbf{r}_j, \\ \frac{1}{|\mathbf{r}_i - \mathbf{R} - \mathbf{r}_j|^3} & \text{otherwise.} \end{cases} \quad [4]$$

The double sum in Eq. 2 can be calculated in advance, since it is dependent on the positions i and j only, making the Hamiltonian computationally equivalent to the case without long-range interactions (Eq. 5):

$$H = -\sum_{i,j} \Pi_{ij} \sigma_i \sigma_j + \frac{1}{2} \sum_{i,j} \Delta_{ij} p(\delta_i) p(\delta_j) \quad [5]$$

where

$$\Pi_{ij} = \sum_{\mathbf{R}} \Pi(\mathbf{r}_i, \mathbf{R} + \mathbf{r}_j), \quad \Delta_{ij} = \sum_{\mathbf{R}} \Delta(\mathbf{r}_i, \mathbf{R} + \mathbf{r}_j) \quad [6, 7]$$

The effective interaction parameters (Eq. 6 and 7) include the attractive nearest neighbor coupling energy as well as the dipole-dipole repulsion between two occupied positions and replicas and need to be calculated only once at the beginning of a MC simulation, which then scales linearly with the number of molecules. This allowed the search of the equilibrium configuration for large unit systems (10^5 adsorption sites, corresponding to a 200×200 nm² surface), thereby approaching the experimental images size. This was useful for direct qualitative/quantitative comparison with experiments and improved accuracy (in fact, the underestimation of the dipolar contribution due to finite system size is minimal in this way).

The bimolecular TBP-TCNQ mixture was represented by fixing the concentration of TCNQ and then “fluxing” some TBP-like particles in the system (by imposing that the system be in chemical equilibrium with an infinite reservoir). In a typical simulated annealing run, the temperature was decreased linearly from 300K to 77K over 10^8 MC steps and then kept at 77 K for further 10^7 steps for equilibration.

The equilibrium structures produced by the model are in excellent qualitative agreement with the experimental observations in the relevant TCNQ:TBP = 3:1 stoichiometry (see Figure 7 and ESI-9(a)). Phase segregation is the expected outcome due to the unfavorable van der Waals TBP-TCNQ mixing; however, the used mix of opposite dipoles with different strengths carried by the two species make the formation of a one-molecule-thick TBP rim around TCNQ islands energetically convenient.

A very different outcome was obtained when simulating neutral TCNQ and TBP particles after switching off all the electrostatic contributions. In this case, our model invariably predicted the formation of two homomolecular aggregates (Figure ESI-9(b)). Finally, we investigated systems in which one molecule only is a dipole carrier. Figure ESI-9(c) shows an equilibrium structure obtained simulating a system where TBP is modeled as charged and TCNQ is kept neutral, while and Figure ESI-9(d) shows the opposite situation. In both cases, the model predicts the formation of a single island of the neutral species and several islands of the charged one (due to electrostatic repulsion). In conclusion, the equilibrium Monte Carlo analysis provides further indication that the experimentally observed aggregation pattern (i.e., TCNQ islets surrounded by a monomolecular TBP rim) requires both molecular species to be charged.

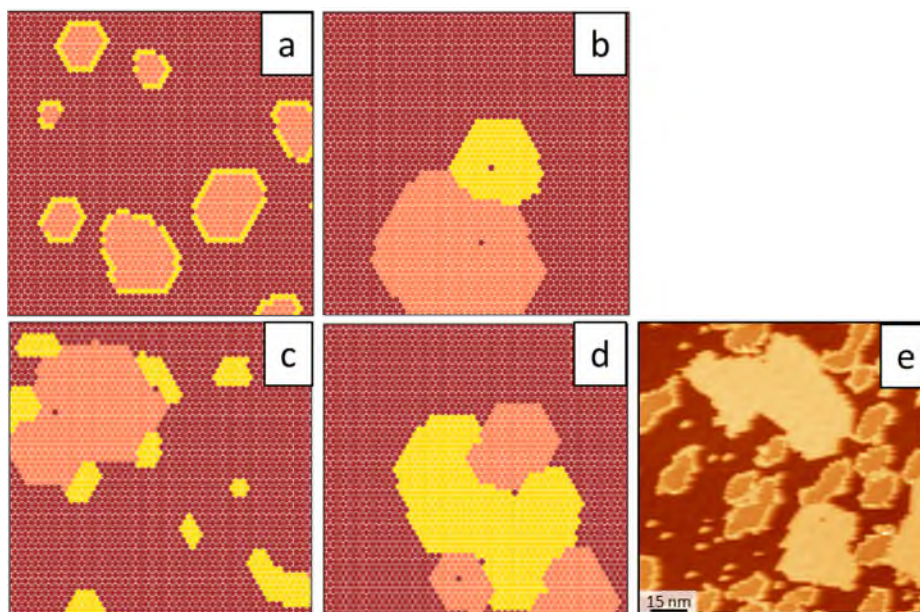


Figure ESI-9: Equilibrium Monte Carlo simulations snapshots of the co-deposition of TBP and TCNQ molecules, obtained by considering: (a) both molecules charged, (b) both neutral, (c) charged TBP and neutral TCNQ and (d) charged TCNQ and neutral TBP. TBP and TCNQ molecules are represented as yellow and pink small hexagons, respectively. The observed experimental assembly is reported in (e) for comparison.

References

1. I. F. Torrente, K. J. Franke and J. I. Pascual, *Int. J. Mass Spectrom.*, 2008, **277**, 269-273.
2. R. Smoluchowski, *Physical Review*, 1941, **60**, 661-674.
3. J. Tersoff and L. M. Falicov, *Phys. Rev. B*, 1981, **24**, 754-764.
4. J. F. Jia, K. Inoue, Y. Hasegawa, W. S. Yang and T. Sakurai, *Phys. Rev. B*, 1998, **58**, 1193-1196.
5. M. M. Kamna, T. M. Graham, J. C. Love and P. S. Weiss, *Surf. Sci.*, 1998, **419**, 12-23.
6. T. Katayama, K. Mukai, S. Yoshimoto and J. Yoshinobu, *Phys. Rev. B*, 2011, **83**, 153403.
7. D. Wegner, R. Yamachika, Y. Wang, V. W. Brar, B. M. Bartlett, J. R. Long and M. F. Crommie, *Nano Lett.*, 2008, **8**, 131-135.
8. T. R. Umbach, I. Fernandez-Torrente, J. N. Ladenthin, J. I. Pascual and K. J. Franke, *J. Phys.: Condens. Matter.*, 2012, **24**, 354003-354008.
9. A. Della Pia, M. Riello, A. Floris, D. Stassen, T. S. Jones, D. Bonifazi, A. De Vita and G. Costantini, *ACS Nano*, 2014, **8**, 12356-12364.
10. W. Erley and H. Ibach, *Surf. Sci.*, 1986, **178**, 565-577.
11. R. Otero, J. M. Gallego, A. L. V. de Parga, N. Martin and R. Miranda, *Adv. Mater.*, 2011, **23**, 5148-5176.
12. V. Sahni and K. P. Bohnen, *Phys. Rev. B*, 1985, **31**, 7651-7661.
13. T.-C. Tseng, C. Urban, Y. Wang, R. Otero, S. L. Tait, M. Alcamí, D. Ecija, M. Trelka, J. Maria Gallego, N. Lin, M. Konuma, U. Starke, A. Nefedov, A. Langner, C. Woell, M. Angeles Herranz, F. Martin, N. Martin, K. Kern and R. Miranda, *Nature Chem.*, 2010, **2**, 374-379.
14. S. Bedwani, D. Wegner, M. F. Crommie and A. Rochefort, *Phys. Rev. Lett.*, 2008, **101**, 216105-216101-216105-216104.
15. C. Wackerlin, C. Iacovita, D. Chylarecka, P. Fesser, T. A. Jung and N. Ballav, *Chem. Commun.*, 2011, **47**, 9146-9148.
16. M. N. Faraggi, N. Jiang, N. Gonzalez-Lakunza, A. Langner, S. Stepanow, K. Kern and A. Arnau, *J. Phys. Chem. C*, 2012, **116**, 24558-24565.
17. N. Abdurakhmanova, A. Floris, T. C. Tseng, A. Comisso, S. Stepanow, A. De Vita and K. Kern, *Nat. Commun.*, 2012, **3**, 940.
18. J. Tersoff and D. R. Hamann, *Phys. Rev. B*, 1985, **31**, 805-813.
19. E. V. Chulkov, V. M. Silkin and P. M. Echenique, *Surf. Sci.*, 1999, **437**, 330-352.
20. G. Tomba, M. Stengel, W.-D. Schneider, A. Baldereschi and A. De Vita, *ACS Nano*, 2010, **4**, 7545-7551.
21. M. Dion, H. Rydberg, E. Schröder, D. C. Langreth and B. I. Lundqvist, *Phys. Rev. Lett.*, 2004, **92**, 246401.
22. R. Rürger and R. Valentí, *Phys. Rev. B*, 2012, **86**, 024431-024431-024431-024435.